JDI Journal of Diabetes Investigation Open access
Official Journal of the Asian Association for the Study of Diabetes
ORIGINAL ARTICLE

CircZNF532 knockdown protects retinal pigment epithelial cells against high glucose-induced apoptosis and pyroptosis by regulating the miR-20b-5p/STAT3 axis

Gao-Hua Liang[1], Yan-Ni Luo[1], Ri-Zhang Wei[1], Jia-Yang Yin[2], Zhi-Liang Qin[1], Li-Li Lu[1], Wen-Hao Ma[1]*

[1]Department of Ophthalmology, The Affiliated Hospital of Youjiang Medical University for Nationalities, Baise, China, and [2]Department of Ophthalmology, The First Affiliated Hospital of Jinan University, Guangzhou, China

Keywords
Diabetic retinopathy, miR-20b-5p, STAT3

***Correspondence**
Wen-Hao Ma
Tel.: +86-0776-2830951
Fax: +86-0776-2830951
Email: mawenhaoeye@163.com

J Diabetes Investig 2022; 13: 781–795

doi: 10.1111/jdi.13722

ABSTRACT

Introduction: The loss of retinal pigment epithelial (RPE) cells is associated with the etiology of diabetic retinopathy (DR). This study investigated the effects of circular RNA ZNF532 (circZNF532) on apoptosis and pyroptosis of RPE cells.

Materials and Methods: Blood samples were collected from patients with DR and healthy volunteers. A human RPE cell line ARPE-19 was induced by high glucose (HG) and assayed for cell viability, apoptosis, and pyroptosis. The binding of miR-20b-5p with circZNF532 and STAT3 was confirmed by a luciferase activity assay. A mouse model of diabetic retinopathy was established.

Results: CircZNF532 and STAT3 were upregulated but miR-20b-5p was downregulated in the serum samples of patients with DR and HG-induced ARPE-19 cells. Elevated miR-20b-5p or CircZNF532 knockdown enhanced proliferation but reduced apoptosis and pyroptosis of ARPE-19 cells. CircZNF532 sponged miR-20b-5p and inhibited its expression. STAT3 was verified as a target of miR-20b-5p. MiR-20b-5p modulated ARPE-19 cell viability, apoptosis, and pyroptosis by targeting STAT3. Mice with STZ-induced diabetes showed elevated expressions of circZNF532 and STAT3 but decreased the level of miR-20b-5p compared with the controls. Knockdown of circZNF532 inhibited apoptosis and pyroptosis in mouse retinal tissues.

Conclusion: CircZNF532 knockdown rescued human RPE cells from HG-induced apoptosis and pyroptosis by regulating STAT3 via miR-20b-5p.

INTRODUCTION

Diabetic retinopathy (DR) is a retinal neurodegenerative disease that can cause vision loss and blindness in people who have diabetes mellitus (DM)[1]. As a common complication of diabetes, DR remains a principal cause of visual impairment among working-age individuals[2] and is associated with a prolonged duration of hypertension and hyperglycemia[3]. During diabetic retinopathy, sustained high-level blood glucose impairs various retinal tissues, including retinal pigment epithelial (RPE) cells, which form a barrier that separates the fenestrated choriocapillaris and the neuronal retina[4]. The breakdown of the RPE barrier plays a causative role in the development of diabetic retinopathy[5]. Hyperglycemia-caused RPE cell apoptosis, a process of programmed cell death mediated by apoptotic caspases, contributes to the progression of diabetic retinopathy[6]. In addition, RPE cell pyroptosis, a form of necrotic and inflammatory programmed cell death induced by inflammatory caspases, is also involved in the development of DR[7]. It is critical to elucidate the mechanisms underlying cell apoptosis and pyroptosis for the treatment of diabetic retinopathy.

The involvement of circular RNAs (circRNAs) has been uncovered in the pathophysiology of diabetes-related complications[8]. CircRNA COL1A2 is reported to augment angiogenesis in DR[9]. Besides, circRNA 0084043 silencing depresses high glucose (HG)-induced RPE cell (ARPE-19 cell) damage in diabetic retinopathy[10]. A previous study discovered that circZNF532

Received 4 March 2021; revised 5 November 2021; accepted 21 November 2021

orchestrated human diabetic vitreous-induced retinal pericyte degeneration and vascular dysfunction[11]. The network consisting of circRNA[12], microRNA (miRNA)[13], and mRNA is highly involved in the progression of diabetic retinopathy[14]. Furthermore, differentially expressed miR-20b-5p has been observed under diabetic conditions[15]. Zhu *et al.* found the association of miR-20b-5p with diabetic retinal vascular dysfunction[16].

MiRNAs play a crucial part in the modulation of gene expression at the posttranscriptional level[17]. Previous data unveiled that miR-20b-5p could bind with STAT3 (encoding signal transducer and activator of transcription 3) and inhibit its expression in human retinoblastoma[18]. STAT3 increases cell pyroptosis by elevating the transcription of the gasdermin C (GSDMC) gene in breast cancer cells[19]. Elevated STAT3 phosphorylation was observed in rats with DR, while STAT3 inhibition alleviated the vision loss in rat models of diabetic retinopathy[20,21].

This study aimed to investigate whether circZNF532 would affect RPE cell pyroptosis in DR via miR-20b-5p and STAT3, thus providing a novel insight into the pathology of pyroptosis during DR.

MATERIALS AND METHODS

Ethical approval

The study was approved by the Ethical Review Committee of The Affiliated Hospital of Youjiang Medical University for Nationalities, following the 1964 Helsinki declaration. Each participant signed informed consent. The animal study was performed following the NIH Guidelines of the Care and Use of Laboratory Animals.

Clinical samples

Fifty-six patients (25 females and 31 males) who were diagnosed with type 2 diabetes mellitus combined with diabetic retinopathy were recruited. Type 2 diabetes mellitus was diagnosed according to the American Diabetes Association diagnostic criteria 2015[22]. The diagnosis of DR was confirmed by best-corrected visual acuity, fundus fluorescein angiography (FFA), and indirect ophthalmoscopy (full ophthalmologic examination)[23]. Among these patients, there were 18 cases with non-proliferative diabetic retinopathy (NPDR), 22 cases with proliferative diabetic retinopathy (PDR), and 16 cases with pre-proliferative diabetic retinopathy (PrePDR). The main manifestations of PrePDR in fundus fluorescein angiography included severe retinal hemorrhage in four quadrants, venous bleeding in two quadrants, and the absence of the capillary perfusion area. The main manifestation of PDR was the proliferation of new vessels[24]. Among 56 patients with diabetic retinopathy, there were 41 cases with diabetic macular edema (DME). Another group consisting of 20 patients (9 females, 11 males) with type 2 diabetes mellitus but without diabetic retinopathy were also enrolled. In addition, 20 healthy volunteers (9 females and 11 males) without systemic or ocular diseases served as normal controls. No participant had cardiovascular disease, peripheral vascular disease, liver or renal dysfunction, or malignancy. Venous blood samples were collected from all subjects following a 12 h fast.

Cell culture and transfection

Human RPE cell line ARPE-19 (ATCC, USA) was cultured in DMEM (Gibco, USA) supplemented with 10% fetal bovine serum (FBS) and maintained in an incubator (5% CO_2) at 37°C. The ARPE-19 cells were exposed to 5 mM [normal glucose (NG)], 10 mM, 15 mM, 20 mM, or 25 mM (HG) of glucose (Sigma-Aldrich, USA) for 72 h. The exposure of cells to high glucose (25 mM) was used to establish the cell model of diabetic retinopathy[25–27]. Short hairpin RNA (shRNA) for circZNF532 (sh-ZNF532), circZNF532 expression vector (oe-ZNF532), miR-20b-5p mimic, miR-20b-5p inhibitor, STAT3 expression vector (oe-STAT3), and their corresponding negative control (NC) (all by GenePharma, China) were introduced into ARPE-19 cells alone or in combination using lipofectamine 2000 reagents (Invitrogen, USA).

Dual-luciferase reporter assay

Bioinformatics analysis provides a binding potential of miR-20b-5p and ZNF532 or STAT3 using Starbase (http://starbase.sysu.edu.cn/). The sequence of ZNF532 or STAT3 3′UTR containing the wild-type (WT) miR-20b-5p binding site was inserted into the pmirGLO luciferase reporter vector (Promega, USA). The mutant-type reporter ZNF532-MUT or STAT3-MUT was also constructed. The ARPE-19 cells were co-transfected with ZNF532-WT or ZNF532-MUT concurrent with miR-20b-5p mimic or NC. STAT3-WT and STAT3-MUT were also prepared and delivered into ARPE-19 cells with miR-20b-5p mimic or NC. After 48 h, the luminescence of firefly luciferase in ARPE-19 cells was determined using a dual-luciferase reporter assay system kit (K801-200, BioVision, USA), and Glomax20/20 luminometer (Promega).

Cell counting kit-8 (CCK-8) assay

The CCK-8 assay was performed to examine ARPE-19 cell proliferation. The ARPE-19 cells were plated in a 96-well plate (5000 cells/well) and CCK-8 was added for 2 h at 37°C. The cell viability was reflected by the optical density (OD) at 450 nm.

3-(4,5-Dimethylthiazol-2-yl)-2,5-diphenyl-2H-tetrazolium bromide (MTT) assay

The ARPE-19 cells were cultured under iso-osmolar medium, hyperosmolar medium (medium containing additional 100 mM NaCl (Na100) or 200 mM sucrose (Su200)), or medium containing 25 mM of glucose for 24 h. Then, 10 μL of MTT solution (5 mg/mL; Serva, Heidelberg, Germany) was added to the cells. After 4 h, the culture supernatants were removed and the absorbance was recorded at 570 nm.

Enzyme-linked immunosorbent assay (ELISA)

The ARPE-19 cell supernatants and mouse retinal tissue lysates were collected for the measurement of IL-1β, IL-18, TNF-α,

and IL-6 using ELISA (Elabscience Biotechnology Co., Ltd, China).

Flow cytometry

The ARPE-19 cells and mouse retinal tissues were resuspended in 500 μL 1 × binding buffer and mixed with Annexin V-FITC (5 μL; Beyotime, China) and propidium iodide (PI, 5 μL; Beyotime) in the dark at 37°C for 20 min. An annexin A flow cytometer (Bio-Rad, USA) and Cell Quest Pro software (BD Biosciences, USA) were used to determine if the cells were viable, apoptotic, or necrotic. A fluorochrome inhibitor of caspase-1 (caspase-1-FLICA) conjunct with PI was analyzed by flow cytometer to determine pyroptotic cells as reported previously[28]. Pyroptotic cells were positive for PI and caspase-1 FLICA.

Animal model

A mouse model of diabetic retinopathy was established by intraperitoneal injection with streptozotocin (STZ) as described previously[9]. Six-week-old male C57BL/6J mice were purchased from (Shanghai Laboratory Animal Center, China) and housed in a controlled environment (22 ± 2°C, 12 h light/dark cycle) with free access to food and water. After 1 week acclimation, the mice were randomly divided into Control, STZ, STZ+sh-NC, and STZ+sh-ZNF532 groups (n = 6 per group). The mice subjected to STZ injection were intraperitoneally administered with STZ at a dose of 60 mg/kg/day for 5 successive days. Mice in the control group were injected with an equal volume of vehicle. The fasting blood glucose was measured once a week. Mice with fasting blood glucose over 300 mg/dL were considered to be diabetic. Intravitreal injection with lentiviral vectors expressing sh-NC or sh-ZNF532 (1 μL of 10^{10} TU/mL) was performed at 4 weeks following STZ injection. After another 4 weeks, all mice were euthanized. The retinal tissues were harvested and prepared for hematoxylin and eosin (H&E) staining. The slides were observed under a light microscope.

Quantitative reverse transcription PCR (qRT-PCR)

Total RNA was extracted from serum, ARPE-19 cells, and mouse retinal tissue lysates using TRIzol reagents (Invitrogen, USA). Complementary DNA (cDNA) was produced using a TaqMan microRNA reverse transcription kit (Applied Biosystems, USA) for miRNA and First Strand cDNA synthesis reverse transcription kit (Applied Biosystems) for mRNA. qRT-PCR was conducted using SYBR Green Master Mix (Applied Biosystems) in the ABI7500 System (Applied Biosystems). The primers (Table 1) were synthesized by GenePharma (China). GAPDH was used as an endogenous control.

Table 1 | The oligonucleotide primers used for PCR amplifications

Target	Primer sequences (5′–3′)
miR-20b-5p	Sense: 5′-GAGCTTATTCATAAAAGT-3′
miR-20b-5p	Antisense: 5′-TCCACGACACGCACTGGATACGAC-3′
U6	Sense: 5′-ATTGGAACGATACAGAGAAGATT-3′
U6	Antisense: 5′-GGAACGCTTCACGAATTTG-3′
circZNF532	Sense: 5′-CAGTTGAAGGCGAAAAGGGC-3′
circZNF532	Antisense: 5′-TGAAGCCAAGGTGGTGGTTT-3′
STAT3	Sense: 5′-CCTGAAGCTGACCCAGGTAG-3′
STAT3	Antisense: 5′-TTCCAAACTGCATCAATGAATC-3′
IL-1β	Sense: 5′-CACCTCTCAAGCAGAGCACAGA-3′
IL-1β	Antisense: 5′-ACGGGTTCCATGGTGAAGTC-3′
IL-18	Sense: 5′-ACCGCAGTAATACGGAGCAT-3′
IL-18	Antisense: 5′-TCTGGGATTCGTTGGCTGTT-3′
IL-6	Sense: 5′-TAGCCTCAATGACGACCTAAG-3′
IL-6	Antisense: 5′-GTGGGGCTGATTGGAAACCT-3′
TNF-α	Sense: 5′-CCGATGGGTTGTACCTTGTC-3′
TNF-α	Antisense: 5′-GGCAGAGAGGAGGTTGACTTT-3′
ASC	Sense: 5′-TTATGGAAGAGTCTGGAGCTGTGG-3′
ASC	Antisense: 5′-AATGAGTGCTTGCCTGTGTTGG-3′
NLRP3	Sense: 5′-CCAGGGCTCTGTTCATTG-3′
NLRP3	Antisense: 5′-CCTTGGCTTTCACTTCG-3′
GAPDH	Sense: 5′-GCACCGTCAAGGCTGAGAAC-3′
GAPDH	Antisense: 5′-TGGTGAAGACGCCAGTGGA-3′

Immunoblotting

The ARPE-19 cells and mouse retinal tissues were lysed in RIPA lysis buffer (Beyotime) and subjected to 10% SDS-PAGE processing and membrane transfer. The primary antibodies against ASC (#67824, Cell Signaling Technology (CST), USA), NLRP3 (#13158, CST), caspase-1 (#24232, CST), pro-caspase-1 (ab179515, Abcam, UK), Bcl-2 (#15071, CST), Bax (#14796, CST), cleaved-caspase-3 (#9661, CST), cleaved-caspase-9 (#20750, CST), vascular endothelial growth factor (VEGF, ab52917, Abcam), and GAPDH (#5174, CST) were added, followed by the addition of secondary antibody with enhanced chemiluminescence (ECL) reagents (BB-3501, Amersham Pharmacia, UK). Acquired immunoblots were photographed using a Bio-Rad Image Analysis System (BIO-RAD, USA), and analyzed with a gel documentation system (Bio-Rad Quantity One Software v4.6.2, USA). The protein expression was normalized to that of GAPDH.

Statistical analysis

All values were obtained from three repeats and are presented as mean ± standard deviation. Statistical comparison was performed in SPSS 21.0 (IBM, USA) using Student's t-test, one-way analysis of variance (ANOVA) with Tukey's adjustments, and repeat measurements ANOVA. A value of $P < 0.05$ indicated statistical significance. The Pearson coefficient was performed for correlation analysis.

RESULTS

Expressions of circZNF532, STAT3, and miR-20b-5p in DR

We first compared the expressions of circZNF532, miR-20b-5p, and STAT3 in diabetic patients with diabetic retinopathy (DR), diabetic patients without DR (D), and healthy controls (HC). circZNF532 and STAT3 were upregulated, while miR-20b-5p was downregulated in the serum samples of patients with

diabetic retinopathy in comparison with diabetic patients without DR and healthy volunteers (Figure 1a). The expressions of circZNF532, miR-20b-5p, and STAT3 were significantly different in HC vs PDR and HC vs PrePDR groups. Moreover, the level of circZNF532 in the PrePDR group was lower than that in patients with PDR, suggesting a severity-dependent change in the expression of circZNF532 (Figure 1b). The comparison between patients with DME and HC showed that circZNF532 and STAT3 were upregulated, while miR-20b-5p was downregulated in patients with DME (Figure 1c). Next, we treated

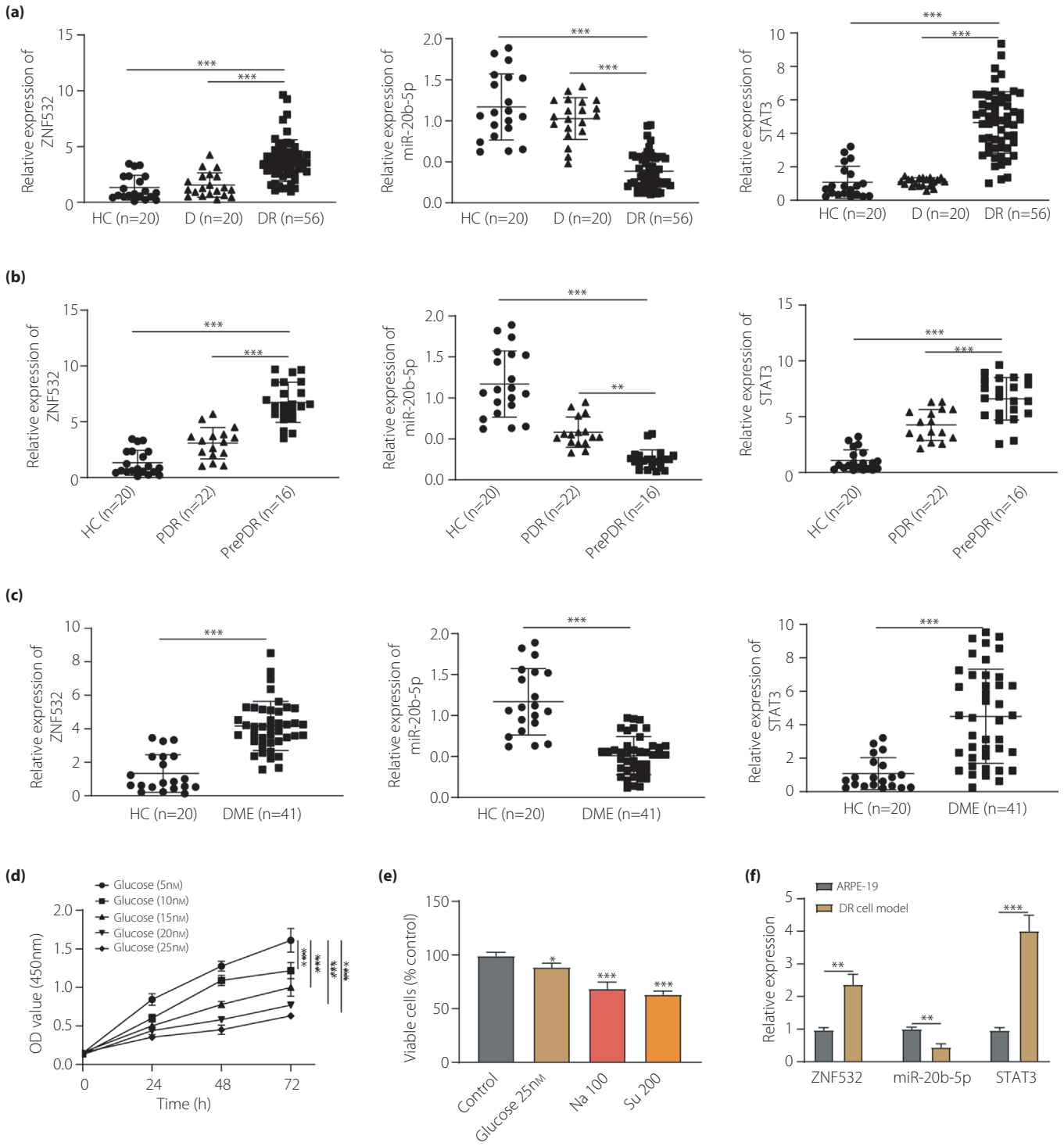

Figure 1 | CircZNF532 and STAT3 were upregulated but miR-20b-5p was downregulated in the serum of patients with diabetic retinopathy and HG-induced ARPE-19 cells. (a–c) Total RNA was extracted from serum samples and the expressions of circZNF532, miR-20b-5p, and STAT3 in different groups of subjects were measured using qRT-PCR. (a) The comparison was made among healthy subjects (HC, $n = 20$), diabetic patients with diabetic retinopathy (DR, $n = 56$), and diabetic patients without diabetic retinopathy (D, $n = 20$). (b) The comparison was made among healthy subjects (HC, $n = 20$), patients with proliferative diabetic retinopathy (PDR, $n = 22$), and patients with preproliferative diabetic retinopathy (PrePDR, $n = 16$). (c) The comparison was made between healthy subjects (HC, $n = 20$) and patients with diabetic macular edema (DME, $n = 41$). (d) ARPE-19 cells were treated with increasing concentrations of glucose for 72 h. Cell proliferation was determined by the CCK-8 assay. (e) ARPE-19 cells were cultured under iso-osmolar medium (Control), hyperosmolar medium (medium containing additional 100 mM NaCl (Na100) or 200 mM sucrose (Su200)), or medium containing 25 mM of glucose for 24 h. Cell viability was measured by the MTT assay. (f) Total RNA was extracted from ARPE-19 cells, and qRT-PCR analysis was used to measure the expressions of circZNF532, miR-20b-5p, and STAT3 in ARPE-19 cells treated with or without high glucose (25 mM glucose) ($n = 3$). * $P < 0.05$. Unpaired Student's *t*-test was used for panel a–c and one-way ANOVA with Tukey's adjustments for panel d.

ARPE-19 cells with varied concentrations of glucose and found that cell proliferation was decreased with the increase in glucose concentration (Figure 1d). Moreover, 25 mM of glucose decreased cell viability. A remarkable decrease in the viability was also observed in cells cultured in hyperosmolar medium (medium containing additional 100 mM NaCl or 200 mM sucrose) (Figure 1e). We also found increased circZNF532 and STAT3 concomitant with declined miR-20b-5p in ARPE-19 cells upon exposure to high glucose (25 mM) compared with normal glucose (5 mM) (Figure 1f).

Elevated miR-20b-5p inhibited ARPE-19 cell apoptosis and pyroptosis

Next, miR-20b-5p mimic and mimic NC were introduced to the ARPE-19 cells. Elevated miR-20b-5p decreased the levels of IL-1β, IL-18, TNF-α, IL-6, ASC, and NLRP3 in cells under high glucose conditions (Figure 2a). The levels of all cytokines were elevated in the ARPE-19 cell supernatants in the presence of HG compared with the group exposed to NG, while miR-20b-5p mimic decreased their levels (Figure 2b). More pyroptotic ARPE-19 cells were observed in HG conditions than in NG conditions; however, decreased numbers of pyroptotic ARPE-19 cells were noted upon miR-20b-5p mimic transfection (Figure 2c). Further analysis of pyroptosis-related proteins revealed that the expressions of caspase-1, ASC, and NLRP3 were elevated in HG-conditioned ARPE-19 cells compared with NG-treated cells, while elevated miR-20b-5p downregulated all these proteins (Figure 2e). More apoptotic ARPE-19 cells were also observed in HG conditions than in NG conditions; however, miR-20b-5p mimic transfection triggered decreased apoptotic ARPE-19 cells (Figure 2d). Immunoblotting analysis revealed elevated cleaved-caspase-3, cleaved-caspase-9, and Bax expressions along with declined Bcl-2 expression in HG conditions relative to cells exposed to NG. Elevated miR-20b-5p reversed the expression patterns in ARPE-19 cells (Figure 2f). The expression of VEGF in ARPE-19 cells cultured under normal or HG conditions and transfected with or without miR-20b-5p was measured. The level of VEGF was increased under HG conditions but decreased by the overexpression of miR-20b-5p (Figure S1A). Finally, HG exposure reduced ARPE-19 cell proliferation, while miR-20b-5p mimic promoted cell viability (Figure 2g). These findings showed that miR-20b-5p increased ARPE-19 cell viability while inhibiting apoptosis and pyroptosis.

CircZNF532 targeted miR-20b-5p

CircRNAs have emerged as miRNA sponges that impair interaction between miRNAs and their target mRNAs[29]. Bioinformatics analysis in Starbase revealed that circZNF532 shared binding sites with miR-20b-5p (Figure 3a). CircZNF532 expression shared negative correlation with miR-20b-5p expression in patients with diabetic retinopathy (Figure 3b). Furthermore, MiR-20b-5p was increased in ARPE-19 cells upon circZNF532 knockdown but declined upon circZNF532 overexpression (Figure 3c). Finally, co-transfection with circZNF532-WT reporter plasmid and miR-20b-5p mimic led to reduced luciferase activity, while the mutant plasmid did not (Figure 3d). These findings indicated that circZNF532 bound with miR-20b-5p and regulated its expression.

CircZNF532 knockdown inhibited ARPE-19 cell apoptosis and pyroptosis by promoting miR-20b-5p

The levels of IL-1β, IL-18, TNF-α, IL-6, ASC, and NLRP3 declined in HG-conditioned ARPE-19 cells upon circZNF532 knockdown, while subsequent miR-20b-5p inhibitor increased their expression levels (Figure 4a,b). sh-ZNF532 transfection reduced ARPE-19 cell pyroptosis in HG conditions; however, combined transfection of sh-ZNF532 and miR-20b-5p inhibitor negated the effect of sh-ZNF532 and promoted the pyroptosis (Figure 4c). Additionally, circZNF532 knockdown led to declined protein expressions of caspase-1, pro-caspase-1, ASC, and NLRP3 in HG conditions. circZNF532 knockdown in ARPE-19 cells continued to be handled with miR-20b-5p inhibitor, while the protein expressions of caspase-1, ASC, and NLRP3 were elevated (Figure 4e). The circZNF532 knockdown also reduced ARPE-19 cell apoptosis in HG conditions. The miR-20b-5p inhibitor negated the effect of sh-ZNF532 and promoted the apoptosis of ARPE-19 cells (Figure 4d). Immunoblotting analysis revealed declined cleaved-caspase-3, cleaved-caspase-9, Bax protein expressions, and elevated Bcl-2 protein expression in HG-conditioned ARPE-19 cells after circZNF532 knockdown. Subsequent miR-20b-5p inhibitor

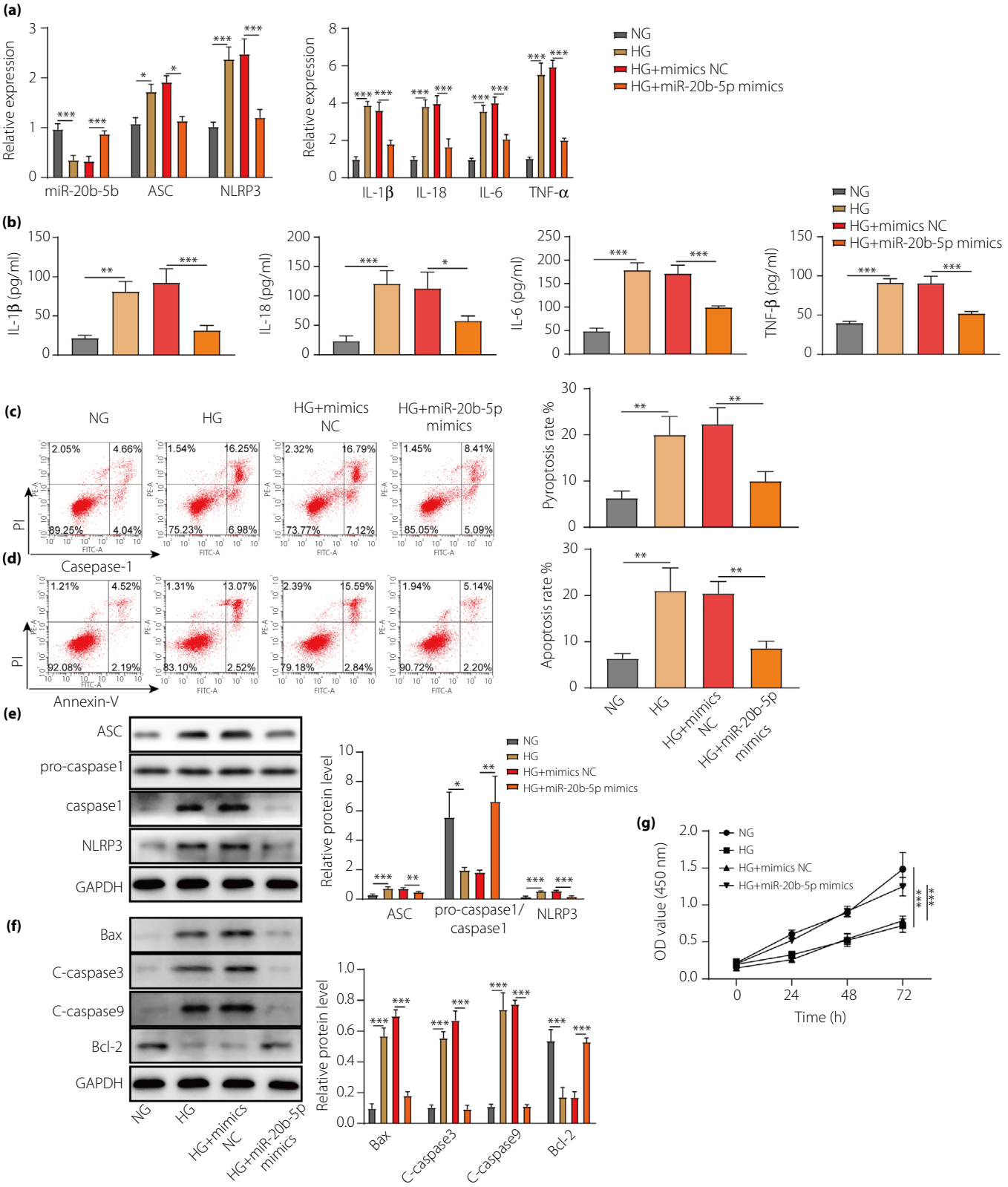

Figure 2 | MiR-20b-5p inhibited ARPE-19 cell apoptosis and pyroptosis following exposure to high glucose. (a) qRT-PCR analysis miR-20b-5p, IL-1β, IL-18, TNF-α, IL-6, ASC, and NLRP3 expression levels in ARPE-19 cells in conditions of high glucose and upon miR-20b-5p mimic transfection. (b) Measurements of IL-1β, IL-18, TNF-α, and IL-6 in ARPE-19 cell culture supernatants in conditions of high glucose and upon miR-20b-5p mimic transfection by ELISA methods. (c) Flow cytometric analysis of caspase-1-FLICA/PI assay was performed to detect pyroptotic ARPE-19 cells in conditions of high glucose and upon miR-20b-5p mimic transfection. (d) Flow cytometric analysis was performed to detect apoptotic ARPE-19 cells in conditions of high glucose and upon miR-20b-5p mimic transfection. (e) Immunoblotting analysis of ASC, pro-caspase-1, caspase-1, and NLRP3 proteins in ARPE-19 cells in conditions of high glucose and upon miR-20b-5p mimic transfection. (f) Immunoblotting analysis of cleaved-caspase-3, cleaved-caspase-9, Bcl-2, and Bax proteins in ARPE-19 cells in conditions of high glucose and upon miR-20b-5p mimic transfection. (g) Examination of ARPE-19 cell proliferation by CCK-8 assay in conditions of high glucose and upon miR-20b-5p mimic transfection. *$P < 0.05$. $n = 3$, one-way ANOVA with Tukey's adjustments was used for panel a–f and repeat measurements ANOVA with Bonferroni corrections for panel g.

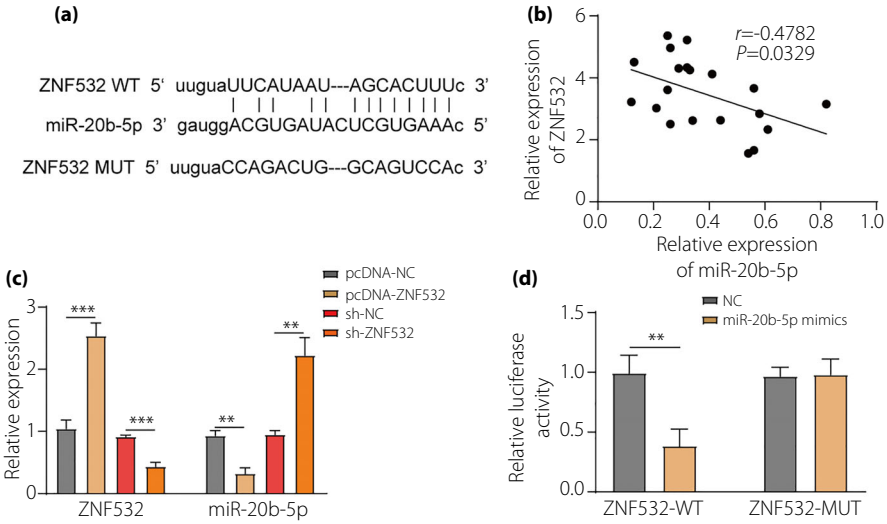

Figure 3 | CircZNF532 targeted miR-20b-5p in ARPE-19 cells. (a) A potential binding site between circZNF532 and miR-20b-5p, predicted by bioinformatic analysis. (b) Pearson coefficient analyzed the correlation between circZNF532 and miR-20b-5p expression in patients with diabetic retinopathy ($n = 20$). (c) qRT-PCR analysis circZNF532 and miR-20b-5p expression levels in circZNF532 knockdown or overexpression ARPE-19 cells ($n = 3$). (d) Dual-Luciferase reporter assay showed circZNF532 binding with miR-20b-5p ($n = 3$). Unpaired Student's test was used for panel c-d.

transfection increased cleaved-caspase-3, cleaved-caspase-9, Bax protein expressions, but reduced Bcl-2 protein expression (Figure 4f). The expression of VEGF in ARPE-19 cells cultured under normal or HG conditions and transfected with or without sh-ZNF532/miR-20b-5p inhibitor was measured. The results showed that HG-induced overexpression of VEGF was suppressed by the transfection with sh-ZNF532, but restored by the downregulated miR-20b-5p (Figure S1B). Finally, circZNF532 knockdown enhanced ARPE-19 cell proliferation, while reduced viability was noted upon subsequent miR-20b-5p inhibitor transfection (Figure 4g). These findings suggested that circZNF532 inhibited miR-20b-5p, reduced viability, and promoted apoptosis and pyroptosis of ARPE-19 cells.

miR-20b-5p targeted STAT3 and inhibited its expression

Bioinformatics analysis in Starbase predicted putative binding sites between miR-20b-5p and STAT3 (Figure 5a). Pearson coefficient analysis showed that STAT3 expression was negatively correlated with miR-20b-5p expression in patients with diabetic retinopathy (Figure 5b). STAT3 was increased in ARPE-19 cells upon miR-20b-5p inhibitor transfection but declined upon miR-20b-5p mimic transfection (Figure 5c,e). The luciferase reporter assay demonstrated that STAT3-WT reporter plasmid, rather than STAT3-MUT reporter plasmid, led to reduced luciferase activity in the presence of miR-20b-5p mimic (Figure 5d). These findings indicated that miR-20b-5p targeted STAT3.

miR-20b-5p inhibited ARPE-19 cell apoptosis and pyroptosis following HG exposure by targeting STAT3

To ascertain whether miR-20b-5p targeting STAT3 affects ARPE-19 cells by regulating their viability, apoptosis, and pyroptosis, miR-20b-5p mimic with oe-STAT3 was delivered into ARPE-19 cells. STAT3 overexpression abated the efficacy of miR-20b-5p mimic and increased the expression levels of IL-1β, IL-18, TNF-α, IL-6, ASC, and NLRP3 in ARPE-19 cells in

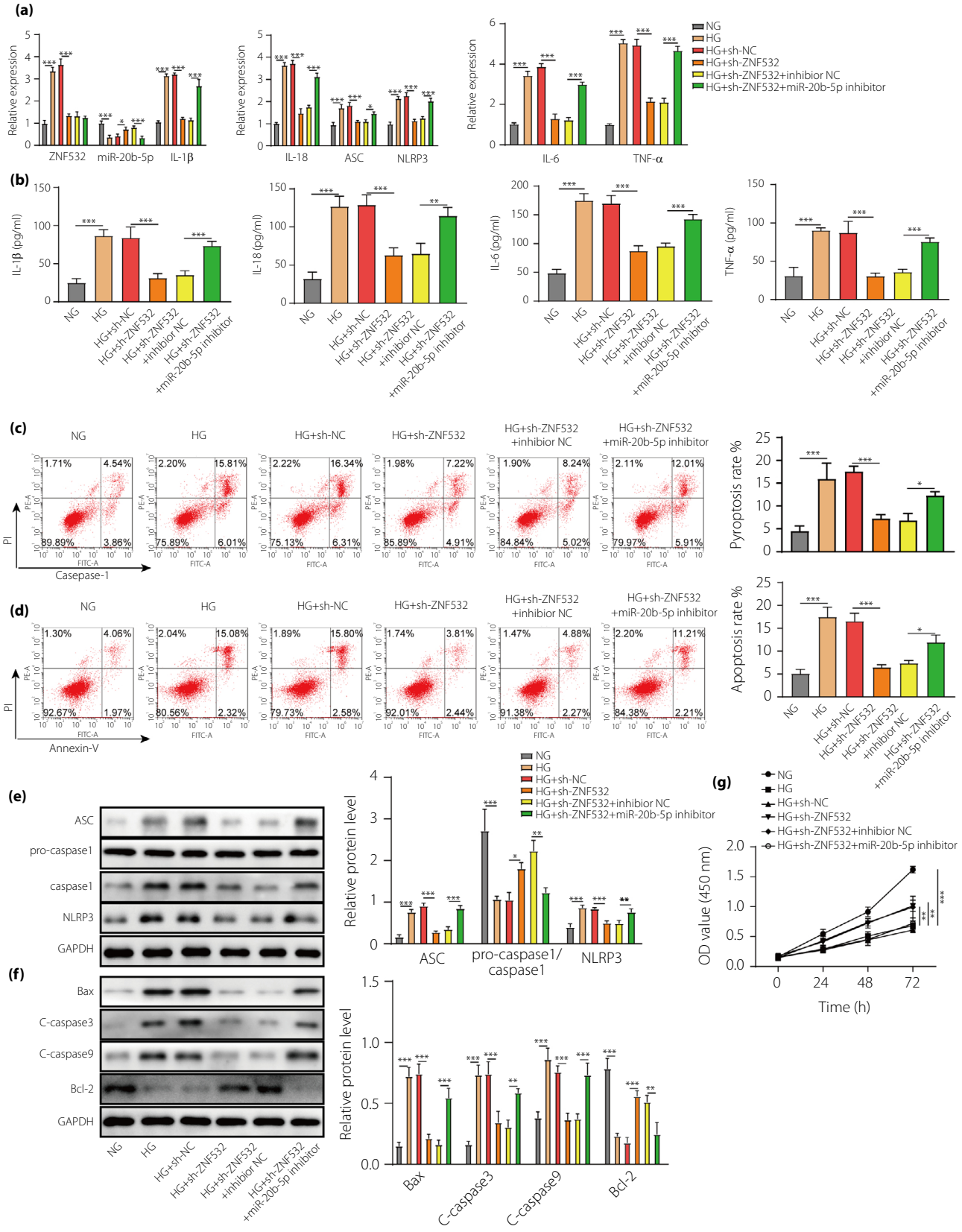

Figure 4 | CircZNF532 knockdown inhibited ARPE-19 cell apoptosis and pyroptosis following high glucose exposure by promoting miR-20b-5p. (a) qRT-PCR analysis circZNF532, miR-20b-5p, IL-1β, IL-18, TNF-α, IL-6, ASC, and NLRP3 expression levels in HG-conditioned ARPE-19 cells following circZNF532 knockdown and/or miR-20b-5p inhibition. (b) Measurements of IL-1β, IL-18, TNF-α, and IL-6 in the culture supernatants of HG-conditioned ARPE-19 cells following circZNF532 knockdown and/or miR-20b-5p inhibition by ELISA methods. (c) Flow cytometric analysis of caspase-1-FLICA/PI assay was performed to detect the pyroptosis of HG-conditioned ARPE-19 cells following circZNF532 knockdown and/or miR-20b-5p inhibition. (d) Flow cytometric analysis was carried out to examine the apoptosis of HG-conditioned ARPE-19 cells following circZNF532 knockdown and/or miR-20b-5p inhibition. (e) Immunoblotting analysis of ASC, pro-caspase-1, caspase-1, and NLRP3 proteins in HG-conditioned ARPE-19 cells following circZNF532 knockdown and/or miR-20b-5p inhibition. (f) Immunoblotting analysis of cleaved-caspase-3, cleaved-caspase-9, Bcl-2, and Bax proteins in HG-conditioned ARPE-19 cells following circZNF532 knockdown and/or miR-20b-5p inhibition. (g) Examination of ARPE-19 cell proliferation by CCK-8 assay in HG-conditioned ARPE-19 cells following circZNF532 knockdown and/or miR-20b-5p inhibition. *$P < 0.05$. $n = 3$, one-way ANOVA with Tukey's adjustments was used for panel a-f and repeat measurements ANOVA with Bonferroni corrections for panel g.

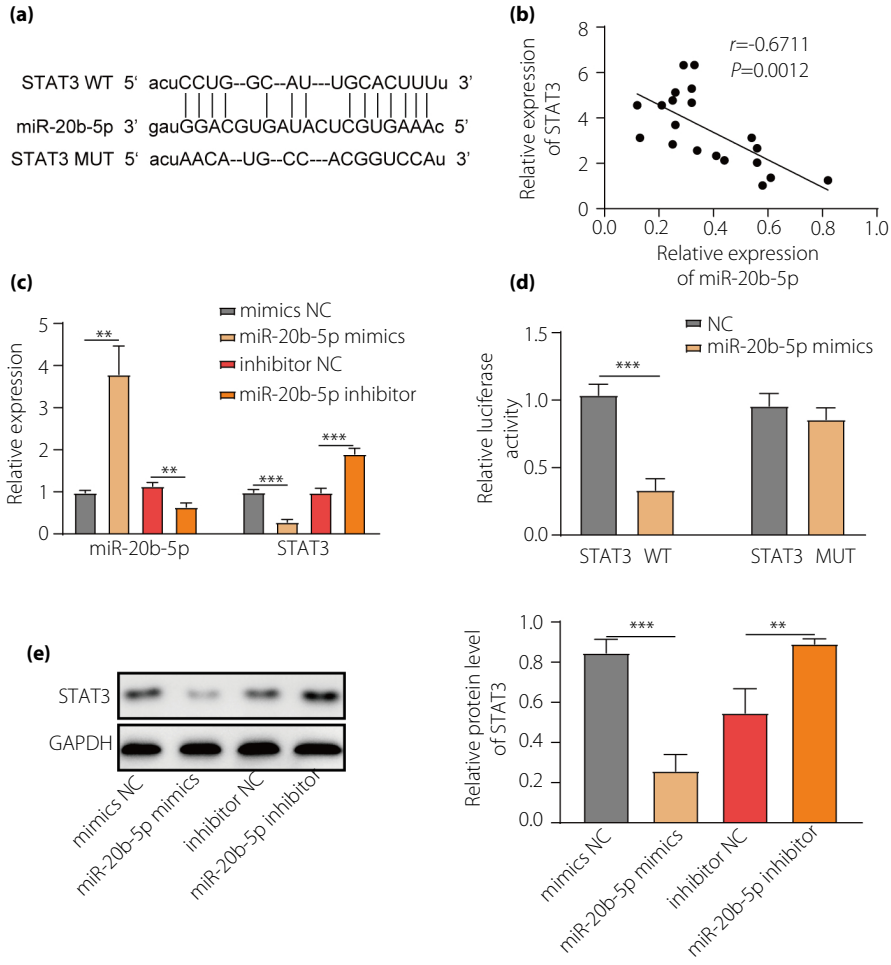

Figure 5 | MiR-20b-5p targeted STAT3 in ARPE-19 cells. (a) Putative miR-20b-5p binding sites in the STAT3 mRNA 3′UTR, predicted by bioinformatic analysis. (b) Pearson coefficient analyzed the correlation between miR-20b-5p and STAT3 expression in patients with diabetic retinopathy ($n = 20$). (c) qRT-PCR analysis miR-20b-5p and STAT3 expression levels in ARPE-19 cells upon miR-20b-5p mimic and inhibitor transfection ($n = 3$). (d) Dual-Luciferase reporter assay showed miR-20b-5p targeting STAT3 ($n = 3$). (e) Immunoblotting analysis of STAT3 protein expression in ARPE-19 cells upon miR-20b-5p mimic and inhibitor transfection ($n = 3$). Unpaired Student's test was used for panel c–e.

HG conditions (Figure 6a,b). STAT3 overexpression also induced pyroptosis in HG-conditioned ARPE-19 cells and led to the loss of miR-20b-5p mimic effects (Figure 6c). Immunoblotting analysis revealed that STAT3 overexpression enhanced protein expressions of caspase-1, pro-caspase-1, ASC, and NLRP3 in HG-conditioned ARPE-19 cells, and the effects

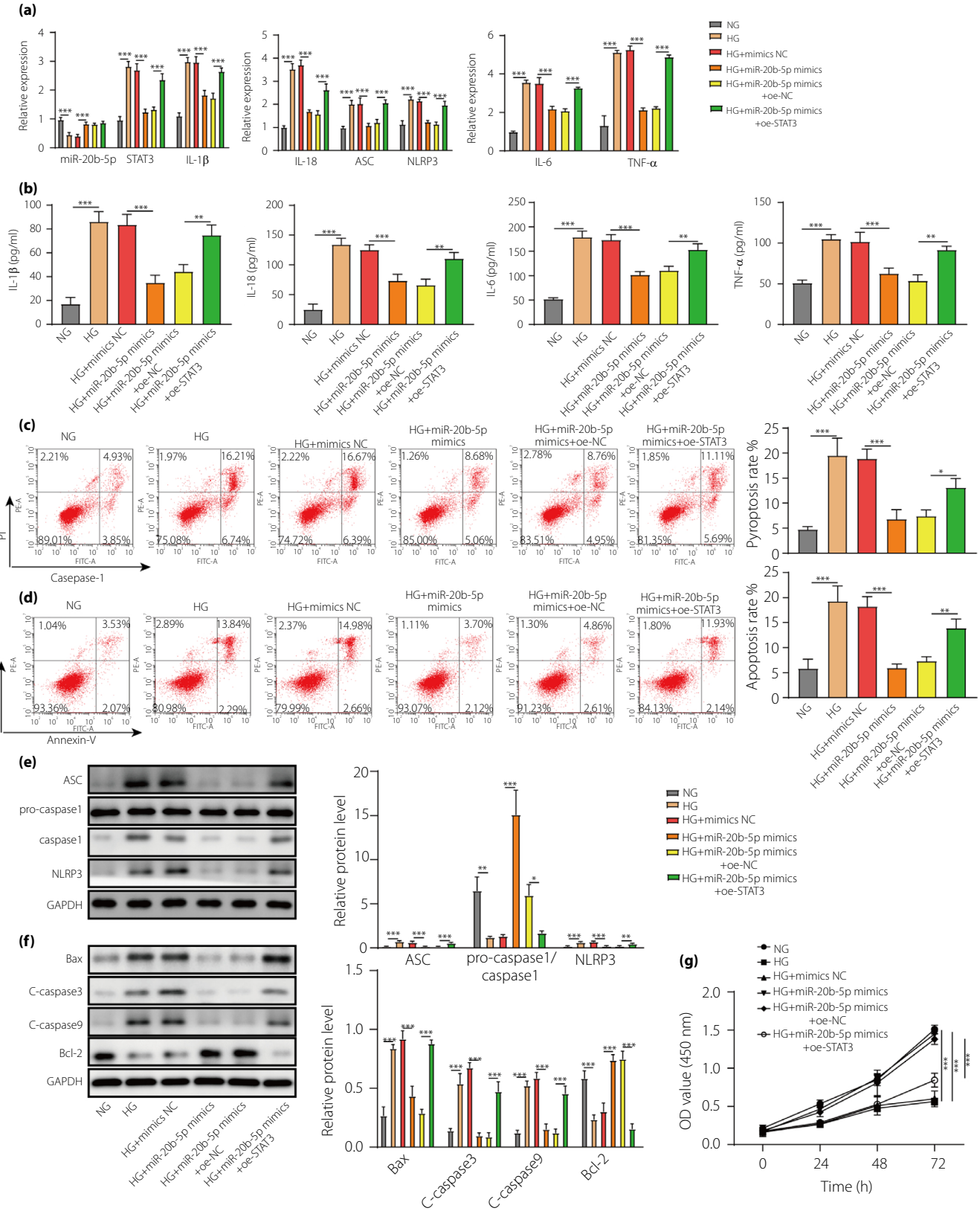

Figure 6 | MiR-20b-5p inhibited ARPE-19 cell apoptosis and pyroptosis following high glucose exposure by targeting STAT3. (a) qRT-PCR analysis miR-20b-5p, STAT3, IL-1β, IL-18, TNF-α, IL-6, ASC, and NLRP3 expression levels in HG-conditioned ARPE-19 cells following miR-20b-5p promotion and/or STAT3 overexpression. (b) Measurements of IL-1β, IL-18,TNF-α and IL-6, in the culture supernatants of HG-conditioned ARPE-19 cells following miR-20b-5p promotion and/or STAT3 overexpression by ELISA methods. (c) Flow cytometric analysis of caspase-1-FLICA/PI assay was performed to detect the pyroptosis of HG-conditioned ARPE-19 cells following miR-20b-5p promotion and/or STAT3 overexpression. (d) Flow cytometric analysis was performed to detect the apoptosis of HG-conditioned ARPE-19 cells following miR-20b-5p promotion and/or STAT3 overexpression. (e) Immunoblotting analysis of ASC, pro-caspase-1, caspase-1, and NLRP3 proteins in HG-conditioned ARPE-19 cells following miR-20b-5p promotion and/or STAT3 overexpression. (f) Immunoblotting analysis of cleaved-caspase-3, cleaved-caspase-9, Bcl-2, and Bax proteins in HG-conditioned ARPE-19 cells following miR-20b-5p promotion and/or STAT3 overexpression. (g) Examination of ARPE-19 cell proliferation by CCK-8 assay in HG-conditioned ARPE-19 cells following miR-20b-5p promotion and/or STAT3 overexpression. *$P < 0.05$. $n = 3$, one-way ANOVA with Tukey's adjustments was used for panel a–f and repeat measurements ANOVA with Bonferroni corrections for panel g.

of miR-20b-5p mimic were partially lost (Figure 6e). STAT3 overexpression also induced HG-induced apoptosis in ARPE-19 cells, while the effects of miR-20b-5p were partially lost (Figure 6d). Immunoblotting analysis revealed STAT3 overexpression enhanced cleaved-caspase-3, cleaved-caspase-9, Bax protein expressions, and reduced Bcl-2 protein expression in HG-conditioned ARPE-19 cells, and as expected, STAT3 overexpression attenuated the effects of miR-20b-5p mimic on the expression of these proteins (Figure 6f). The expression of VEGF in cells cultured under normal or HG conditions and transfected with or without miR-20b-5p mimic/oe-STAT3 was measured. The HG-induced overexpression of VEGF was suppressed by the transfection with miR-20b-5p mimic but restored by the overexpression of STAT3 (Supplementary Figure 1a). Finally, the CCK-8 assay showed that STAT3 overexpression inhibited the proliferation of HG-conditioned ARPE-19 cells and reversed miR-20b-5p mimic effects (Figure 6g). These findings suggested that miR-20b-5p promoted ARPE-19 cell viability while it reduced apoptosis and pyroptosis by targeting STAT3.

CircZNF532 knockdown protected mice against DR via the miR-20b-5p/STAT3 axis

To examine the effect of circZNF532 on diabetic retinopathy *in vivo*, we established a mouse model of diabetic retinopathy. The downregulation of circZNF532 in mice was achieved by injecting the mice with lentiviral vectors expressing sh-ZNF532. Diabetic mice showed elevated mRNA expressions of circZNF532, STAT3, IL-1β, IL-18, TNF-α, IL-6, ASC, and NLRP3, but a decreased the level of miR-20b-5p in comparison with the controls. The downregulation of circZNF532, however, markedly reversed these changes in diabetic mice (Figure 7a). The delivery of lentivirus expressing sh-ZNF532 also effectively inhibited the upregulation of cytokines in diabetic mice (Figure 7b). Histological examination showed that the retinal cells of STZ-treated mice were in an irregular and disordered arrangement compared with the control group, while these changes were alleviated by circZNF532 knockdown (Figure 7c). Furthermore, circZNF532 knockdown inhibited apoptosis (Figure 7d) and pyroptosis (Figure 7e) in the retinal tissues of DR mice. The expressions of caspase-1, ASC, and NLRP3 were elevated in diabetic mice, but this effect was eliminated by the downregulation of circZNF532 (Figure 7f). Moreover, the injection with lentivirus expressing sh-ZNF532 led to decreased expressions of Bax, cleaved-caspase-3, and cleaved-caspase-9, and an elevated Bcl-2 protein level in diabetic mice (Figure 7g). Taken together, these findings implied that the downregulation of circZNF532 protected mice against diabetic retinopathy via regulating the miR-20b-5p/STAT3 axis.

DISCUSSION

Diabetic retinopathy causes damage in the retina owing to a sustained high blood sugar level[30]. The dysfunction of RPE cells has emerged as a contributor to the pathogenesis of diabetic retinopathy[31]. Pyroptosis and apoptosis are two distinct forms of programmed cell death involved in diabetic retinopathy[32,33]. High glucose has been shown to promote RPE apoptosis and death, and eventually causes pathogenesis of diabetic retinopathy[34]. Our study provided evidence that circZNF532 promoted upregulation of STAT3 expression by inhibiting miR-20b-5p, thereby inducing diabetic retinal cell pyroptosis and apoptosis.

Our study first showed that 25 mM of glucose partially decreased the viability of cells, while a remarkable decrease in the viability was observed in cells cultured in hyperosmolar medium, which was consistent with previous studies[25,26]. These findings suggested that a slight increase in osmolality did not significantly affect the cells. Then, we observed that silencing of circZNF532 or overexpression of miR-20b-5p elevated the viability but lowered the apoptosis and pyroptosis of HG-induced ARPE-19 cells. CircRNAs, such as circRNA 0002570, were differentially expressed in DR[35]. CircRNAs function as a modulator of gene expression by orchestrating miRNA functions[36]. In our study, circZNF532 was upregulated during conditions of diabetic retinopathy and it bound to miR-20b-5p to downregulate its expression. Coinciding with our findings, Zhou *et al.* elaborated that miR-20b-5p diminished hypoxia-induced apoptosis in cardiomyocytes via the HIF-1α/NF-κB pathway[37]. Additionally, Zhen *et al.* provided evidence that miR-20b-5p overexpression promoted the viability of propofol-preconditioned endothelial cells and inhibited the autophagy and apoptosis in hypoxia-reoxygenation-induced injury[38].

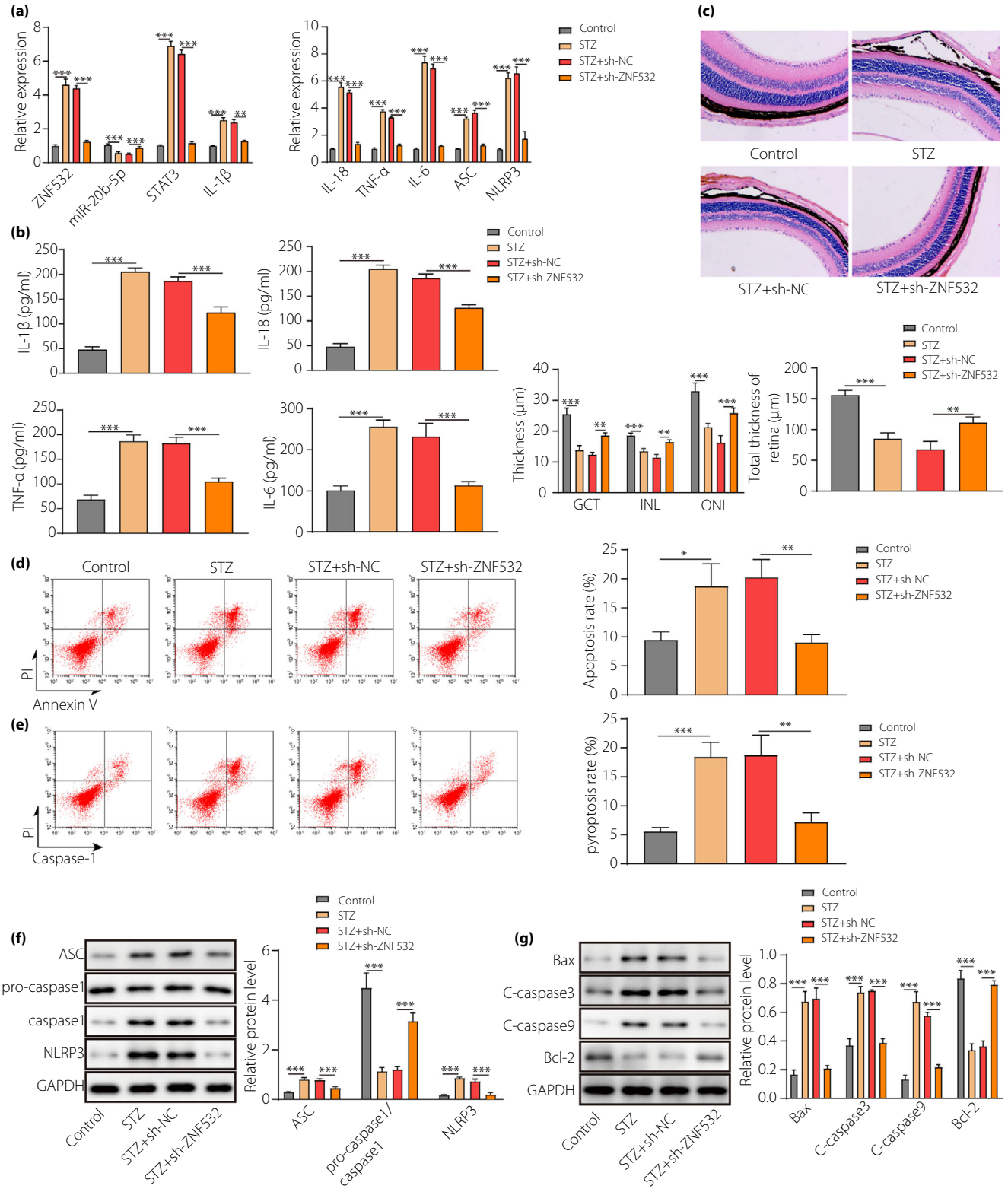

Pyroptosis, an inflammatory form of cell death, is mediated by various inflammasomes, resulting in gasdermin D cleavage and inactive cytokine production, such as IL-18 and IL-1β[39].

NLRP3 activation assumed a critical role in pyroptosis and in the development of diabetes[40]. ASC is widely researched as an adaptor protein correlating to inflammasome assembly and

Figure 7 | Effect of circZNF532 knockdown in a mouse model of diabetic retinopathy. A mouse model of diabetic retinopathy was established by intraperitoneal injection of C57BL/6J mice with STZ. The control group was intraperitoneally injected with an equal volume of vehicle. Diabetic mice were then administered with or without lentiviral vectors expressing sh-NC or sh-ZNF532 via intravitreal injection. (a) The expressions of circZNF532, miR-20b-5p, STAT3, IL-1β, IL-18, TNF-α, IL-6, ASC, and NLRP3 were measured by qRT-PCR. (b) The protein levels of IL-1β, IL-18, TNF-α, and IL-6 were determined by ELISA. (c) The H&E staining was used to assess the pathological changes in mouse retinal tissues. (d) The apoptosis in retinal tissues was detected by flow cytometry. (e) The pyroptosis in retinal tissues was detected by flow cytometry. (f) The expressions of pyroptosis-related proteins, including ASC, pro-caspase-1, caspase-1, and NLRP3 in retinal tissues were measured by Western blot. (g) The expressions of apoptosis-related proteins, including Bax, cleaved-caspase-3, cleaved-caspase-9, and Bcl-2 in retinal tissues were analyzed by Western blot.

pyroptosis[41]. Activated caspase-1 was also suggested as driving gasdermin D to cleavage causing pyroptosis[42]. Our data revealed that IL-1β, IL-18, ASC, NLRP3, and caspase-1 expression were reduced, and the pyroptosis rate also declined in HG-induced ARPE-19 cells after circZNF532 silencing or miR-20b-5p overexpression. These findings were also observed in the mouse model of diabetic retinopathy.

Tang *et al.* revealed that miR-20b-5p targeted and repressed STAT3 in human fetal airway smooth muscle cells[43]. Our study elaborated that miR-20b-5p downregulated STAT3 in ARPE-19 cells. Also, STAT3 was overexpressed in DR and led to a decline in cell viability and to an increase in apoptosis and pyroptosis in HG-induced ARPE-19 cells. Consistently, a previous study reported STAT3 overexpression in rats with DR[20]. Moreover, STAT3 inhibition reduced retinal endothelial cell apoptosis in high glucose conditions[44]. Similarly, STAT3 downregulation caused an increase in viability but a decrease in apoptosis in HC-induced ARPE-19 cells[45]. The VEGF is a downstream effector of the STAT3 pathway, which plays a crucial role in diabetic retinopathy by inducing vascular proliferation, mediating increased vascular permeability, and facilitating pathological angiogenesis[9,46]. The anti-VEGF treatment has been used for patients with proliferative diabetic retinopathy but is limited by major ocular adverse effects[47]. Here, we found that the expression of VEGF was upregulated under high glucose conditions, which was consistent with the study by Maugeri *et al*[48]. Moreover, HG-induced overexpression of VEGF was suppressed by the transfection with sh-ZNF532 or miR-20b-5p mimic but restored by the overexpression of STAT3.

In summary, our study reveals that overexpressed circZNF532 potentially exacerbates the progression of diabetic retinopathy by impairing the inhibitory effects of miR-20b-5p on STAT3, which provides a new perspective for the pathogenesis of diabetic retinopathy and supports future investigation of the circZNF532/miR-20b-5p/STAT3 axis as a potential therapeutic target for diabetic retinopathy.

ACKNOWLEDGMENTS

We would like to give our sincere gratitude to the reviewers for their constructive comments. This work was supported by Natural Science Foundation of Guangxi (Grant/Award number: 2020GXNSFAA259054), and The First Batch of High-level Talent Scientific Research Projects of the Affiliated Hospital of Youjiang Medical University for Nationalities in 2019 (Grant/Award number: R20196340 & Y20196304).

DISCLOSURE

The authors declare that there is no conflict of interest.
Approval of the research protocol: The study protocol was approved by the Ethical Review Committee of The Affiliated Hospital of Youjiang Medical University for Nationalities.
Informed Consent: Each participant signed the informed consent documentation prior to serum sample collection.
Approval date of Registry and the Registration No. of the study/trial: N/A.
Animal Studies: The animal study was performed according to the NIH Guidelines of the Care and Use of Laboratory Animals.

ETHICAL APPROVAL

The study was approved by the Ethical Review Committee of The Affiliated Hospital of Youjiang Medical University for Nationalities, following the 1964 Helsinki declaration. Each participant signed informed consent. The animal study was performed following the NIH Guidelines of the Care and Use of Laboratory Animals.

CONSENT FOR PUBLICATION

Informed consent was obtained from study participants.

DATA AVAILABILITY STATEMENT

All data generated or analyzed during this study are included in this article. The datasets used and/or analyzed during the current study are available from the corresponding author on reasonable request.

REFERENCES

1. Nentwich MM, Ulbig MW. Diabetic retinopathy – ocular complications of diabetes mellitus. *World J Diabetes* 2015; 6: 489–499.
2. Yuan YY, Xie KX, Wang SL, *et al.* Inflammatory caspase-related pyroptosis: mechanism, regulation and therapeutic potential for inflammatory bowel disease. *Gastroenterol Rep* 2018; 6: 167–176.
3. Wong TY, Cheung CM, Larsen M, *et al.* Diabetic retinopathy. *Nat Rev Dis Primers* 2016; 2: 16012.

4. Yu X, Liu Q, Wang X, *et al*. 7,8-Dihydroxyflavone ameliorates high-glucose induced diabetic apoptosis in human retinal pigment epithelial cells by activating TrkB. *Biochem Biophys Res Commun* 2018; 495: 922–927.
5. Xu HZ, Song Z, Fu S, *et al*. RPE barrier breakdown in diabetic retinopathy: seeing is believing. *J Ocul Biol Dis Infor* 2011; 4(1–2): 83–92.
6. Liu R, Li X, Zhang X. Dexmedetomidine protects high-glucose induced apoptosis in human retinal pigment epithelial cells through inhibition on p75(NTR). *Biomed Pharmacother* 2018; 106: 466–471.
7. Zha X, Xi X, Fan X, *et al*. Overexpression of METTL3 attenuates high-glucose induced RPE cell pyroptosis by regulating miR-25-3p/PTEN/Akt signaling cascade through DGCR8. *Aging* 2020; 12: 8137–8150.
8. Zhang JR, Sun HJ. Roles of circular RNAs in diabetic complications: from molecular mechanisms to therapeutic potential. *Gene* 2020; 763: 145066.
9. Zou J, Liu KC, Wang WP, *et al*. Circular RNA COL1A2 promotes angiogenesis via regulating miR-29b/VEGF axis in diabetic retinopathy. *Life Sci* 2020; 256: 117888.
10. Li Y, Cheng T, Wan C, *et al*. circRNA_0084043 contributes to the progression of diabetic retinopathy via sponging miR-140-3p and inducing TGFA gene expression in retinal pigment epithelial cells. *Gene* 2020; 747: 144653.
11. Jiang Q, Liu C, Li C-P, *et al*. Circular RNA-ZNF532 regulates diabetes-induced retinal pericyte degeneration and vascular dysfunction. *J Clin Investig* 2020; 130: 3833–3847.
12. He M, Wang W, Yu H, *et al*. Comparison of expression profiling of circular RNAs in vitreous humour between diabetic retinopathy and non-diabetes mellitus patients. *Acta Diabetol* 2020; 57: 479–489.
13. Shafabakhsh R, Aghadavod E, Mobini M, *et al*. Association between microRNAs expression and signaling pathways of inflammatory markers in diabetic retinopathy. *J Cell Physiol* 2019; 234: 7781–7787.
14. Li W, Jin L, Cui Y, *et al*. Bone marrow mesenchymal stem cells-induced exosomal microRNA-486-3p protects against diabetic retinopathy through TLR4/NF-kappaB axis repression. *J Endocrinol Investig* 2021; 44: 1193–1207.
15. Hromadnikova I, Kotlabova K, Dvorakova L, *et al*. Diabetes mellitus and cardiovascular risk assessment in mothers with a history of gestational diabetes mellitus based on postpartal expression profile of MicroRNAs associated with diabetes mellitus and cardiovascular and cerebrovascular diseases. *Int J Mol Sci* 2020; 21: 2437.
16. Zhu KE, Hu X, Chen H, *et al*. Downregulation of circRNA DMNT3B contributes to diabetic retinal vascular dysfunction through targeting miR-20b-5p and BAMBI. *EBioMedicine* 2019; 49: 341–353.
17. Lu TX, Rothenberg ME. MicroRNA. *J Allergy Clin Immunol* 2018; 141: 1202–1207.
18. Wang L, Zhang Y, Xin X. Long non-coding RNA MALAT1 aggravates human retinoblastoma by sponging miR-20b-5p to upregulate STAT3. *Pathol Res Pract* 2020; 216: 152977.
19. Hou J, Zhao R, Xia W, *et al*. PD-L1-mediated gasdermin C expression switches apoptosis to pyroptosis in cancer cells and facilitates tumour necrosis. *Nat Cell Biol* 2020; 22: 1264–1275.
20. Xu C, Liu GD, Feng L, *et al*. Identification of O-GlcNAcylation modification in diabetic retinopathy and crosstalk with phosphorylation of STAT3 in retina vascular endothelium cells. *Cell Physiol Biochem* 2018; 49: 1389–1402.
21. Vanlandingham PA, Nuno DJ, Quiambao AB, *et al*. Inhibition of Stat3 by a small molecule inhibitor slows vision loss in a rat model of diabetic retinopathy. *Investig Ophthalmol Vis Sci* 2017; 58: 2095–2105.
22. American DA. Diagnosis and classification of diabetes mellitus. *Diabetes Care* 2012; 35: S64–71.
23. Shaker OG, Abdelaleem OO, Mahmoud RH, *et al*. Diagnostic and prognostic role of serum miR-20b, miR-17-3p, HOTAIR, and MALAT1 in diabetic retinopathy. *IUBMB Life* 2019; 71: 310–320.
24. Wang S, Zuo Y, Wang N, *et al*. Fundus fluorescence angiography in diagnosing diabetic retinopathy. *Pak J Med Sci* 2017; 33: 1328–1332.
25. Libert S, Willermain F, Weber C, *et al*. Involvement of TonEBP/NFAT5 in osmoadaptative response of human retinal pigmented epithelial cells to hyperosmolar stress. *Mol Vis* 2016; 22: 100–115.
26. Hollborn M, Ackmann C, Kuhrt H, *et al*. Osmotic and hypoxic induction of the complement factor C9 in cultured human retinal pigment epithelial cells: regulation of VEGF and NLRP3 expression. *Mol Vis* 2018; 24: 518–535.
27. Yang Z, Hu H, Zou Y, *et al*. miR-7 reduces high glucose induced-damage via HoxB3 and PI3K/AKT/mTOR signaling pathways in retinal pigment epithelial cells. *Curr Mol Med* 2020; 20: 372–378.
28. Gu C, Draga D, Zhou C, *et al*. miR-590-3p inhibits pyroptosis in diabetic retinopathy by targeting NLRP1 and inactivating the NOX4 signaling pathway. *Investig Ophthalmol Vis Sci* 2019; 60: 4215–4223.
29. Kristensen LS, Andersen MS, Stagsted LVW, *et al*. The biogenesis, biology and characterization of circular RNAs. *Nat Rev Genet* 2019; 20: 675–691.
30. Peng JJ, Xiong SQ, Ding LX, *et al*. Diabetic retinopathy: focus on NADPH oxidase and its potential as therapeutic target. *Eur J Pharmacol* 2019; 853: 381–387.
31. Ran Z, Zhang Y, Wen X, *et al*. Curcumin inhibits high glucose induced inflammatory injury in human retinal pigment epithelial cells through the ROSPI3K/AKT/mTOR signaling pathway. *Mol Med Rep* 2019; 19: 1024–1031.
32. Peng QH, Tong P, Gu LM, *et al*. Astragalus polysaccharide attenuates metabolic memory-triggered ER stress and apoptosis via regulation of miR-204/SIRT1 axis in retinal pigment epithelial cells. *Biosci Rep* 2020; 40: BSR20192121.

33. Gan J, Huang M, Lan G, *et al*. High glucose induces the loss of retinal pericytes partly via NLRP3-caspase-1-GSDMD-mediated pyroptosis. *Biomed Res Int* 2020; 2020: 4510628.
34. Zhang Y, Xi X, Mei Y, *et al*. High-glucose induces retinal pigment epithelium mitochondrial pathways of apoptosis and inhibits mitophagy by regulating ROS/PINK1/Parkin signal pathway. *Biomed Pharmacother* 2019; 111: 1315–1325.
35. Liu G, Zhou S, Li X, *et al*. Inhibition of hsa_circ_0002570 suppresses high-glucose-induced angiogenesis and inflammation in retinal microvascular endothelial cells through miR-1243/angiomotin axis. *Cell Stress Chaperones* 2020; 25: 767–777.
36. Ebbesen KK, Hansen TB, Kjems J. Insights into circular RNA biology. *RNA Biol* 2017; 14: 1035–1045.
37. Zhou Z, Chen S, Tian Z, *et al*. miR-20b-5p attenuates hypoxia-induced apoptosis in cardiomyocytes via the HIF-1alpha/NF-kappaB pathway. *Acta Biochim Biophys Sin* 2020; 52: 927–934.
38. Zhen W, Hui D, Wenying S, *et al*. MicroRNA-20b-5p regulates propofol-preconditioning-induced inhibition of autophagy in hypoxia-and-reoxygenation-stimulated endothelial cells. *J Biosci* 2020; 45: 35.
39. Fang Y, Tian S, Pan Y, *et al*. Pyroptosis: a new frontier in cancer. *Biomed Pharmacother* 2020; 121: 109595.
40. Yu ZW, Zhang J, Li X, *et al*. A new research hot spot: the role of NLRP3 inflammasome activation, a key step in pyroptosis, in diabetes and diabetic complications. *Life Sci* 2020; 240: 117138.
41. Agrawal I, Jha S. Comprehensive review of ASC structure and function in immune homeostasis and disease. *Mol Biol Rep* 2020; 47: 3077–3096.
42. Platnich JM, Muruve DA. NOD-like receptors and inflammasomes: a review of their canonical and non-canonical signaling pathways. *Arch Biochem Biophys* 2019; 670: 4–14.
43. Tang J, Luo L. MicroRNA-20b-5p inhibits platelet-derived growth factor-induced proliferation of human fetal airway smooth muscle cells by targeting signal transducer and activator of transcription 3. *Biomed Pharmacother* 2018; 102: 34–40.
44. Ye EA, Steinle JJ. miR-146a suppresses STAT3/VEGF pathways and reduces apoptosis through IL-6 signaling in primary human retinal microvascular endothelial cells in high glucose conditions. *Vision Res* 2017; 139: 15–22.
45. Wan W, Wan W, Long Y, *et al*. Physcion 8-O-beta-glucopyranoside exerts protective roles in high glucose-induced diabetic retinopathy via regulating lncRNA NORAD/miR-125/STAT3 signalling. *Artif Cells Nanomed Biotechnol* 2020; 48: 463–472.
46. Witmer AN, Vrensen GF, Van Noorden CJ, *et al*. Vascular endothelial growth factors and angiogenesis in eye disease. *Prog Retin Eye Res* 2003; 22: 1–29.
47. Zhao Y, Singh RP. The role of anti-vascular endothelial growth factor (anti-VEGF) in the management of proliferative diabetic retinopathy. *Drugs Context* 2018; 7: 212532.
48. Maugeri G, Bucolo C, Drago F, *et al*. Attenuation of high glucose-induced damage in RPE cells through p38 MAPK signaling pathway inhibition. *Front Pharmacol* 2021; 12: 684680.

SUPPORTING INFORMATION

Additional supporting information may be found online in the Supporting Information section at the end of the article.

Figure S1 | The expression of VEGF in ARPE-19 cells. (a) Western blot analysis of VEGF in ARPE-19 cells in high glucose conditions and upon miR-20b-5p mimic/oe-STAT3 transfection. (b) Western blot analysis of VEGF in ARPE-19 cells in high glucose conditions and upon sh-ZNF532/miR-20b-5p inhibitor transfection.